Progress In Electromagnetics Research C, Vol. 117, 129–143, 2021

MIMO Antenna for N48, N77, N78 5G Applications

Walaa M. Hassan, Khalid M. Ibrahim*, and Ahmed M. Attiya

Abstract—This paper presents a MIMO antenna system composed of eight wideband horizontal dual-loop antenna elements. Each dual-loop antenna is printed on both sides of a smart phone board. The unit element antenna is designed to operate in the frequency range from 3.2 GHz to 5 GHz. The performance of the MIMO system is then analyzed. The performance of the obtained MIMO system in the frequency range from 3.2 GHz to 4.8 GHzis characterized by input reflection coefficient which is less than −6 dB for all antenna elements, and the isolation between the elements is larger than 15 dB. The total efficiency is greater than 55% over the entire band (3.2–4.8 GHz). Parameters of the multichannel antennas including envelope correlation coefficient (ECC), diversity gain (DG), and channel capacity loss (CLL) are analyzed to evaluate the performance of the MIMO system. The effect of the human hand and head on the performance of this MIMO antenna is also investigated. In addition, the effect of the radiated fields on the human body is also studied. The Specific Absorption Rate (SAR) value is found to be less than 0.8 W/kg. The MIMO system antenna is fabricated and measured. Good agreements are obtained between the simulated and measured parameters. The proposed MIMO system is applicable to the 5G N48, N77, and N78 bands.

1. INTRODUCTION

Multiple-input multiple-output (MIMO) antenna system based on multi-antennas is one of the main technologies for 5G operation [1, 2]. Applying the MIMO technology into a smartphone can achieve large channel capacity, high transmission rate, and high reliability. However, arranging a large number of antennas into a limited space of the smartphone leads to deteriorated isolation between antenna elements and reduces their antenna efficiencies. The quality of mobile communication system can be improved by using a MIMO antenna system [3]. Therefore, loading multiple antennas into a smartphone for 5G communication is presently a challenging topic for antenna engineers.

Compact size and light weight of the smartphone are important requirements in its design. To achieve these requirements, it is required to design antenna with a smaller volume. In recent years, different antenna arrays for 3G/LTE MIMO smartphones have been reported [4–20]. In [4], a hybrid 4G/5G MIMO antenna was presented. The 4G antenna module was used to cover the GSM850/900/1800/1900, UMTS2100, and LTE2300/2500 operating bands, while the 5G antenna module was used to cover the band (3.4–3.6 GHz). Single frequency MIMO systems operating in the 2.6 GHz band (2550–2650 MHz) were proposed in [5, 6]. A square loop radiating strip with orthogonal polarization was used in [5], while in [6] hybrid antenna array elements (C-shaped coupled-fed and L-shaped monopole slot) were used to enhance the port isolation and reduce correlation between antennas. Other Single frequency MIMO systems operating at 3.5 GHz were investigated in [7, 8]. A dual-band MIMO system was achieved by using inverted-F antennas (IFAs) in [9] and a dual inverted-F/loop antennas in [10]. Another design for a dual-band MIMO system 3.5/5 GHz was reported in [11] by using a folded monopole and a gap-coupled loop branch on the upper and bottom sides of the system

Received 26 September 2021, Accepted 8 December 2021, Scheduled 29 December 2021
* Corresponding author: Khalid M. Ibrahim (khaledmus@gmail.com).
The authors are with the Electronics Research Institute (ERI), El-Nozha El-Gadida, Cairo 11843, Egypt.

circuit board, respectively. The design of long term evolution (LTE) band 42, 43, and 46 MHz MIMO system was achieved in [12, 13]. In [12], three different antennas were presented, inverted π-shaped antenna, longer inverted L-shaped open slot antenna, and shorter inverted L-shaped open slot antenna. In [13], T-shaped coupled-fed slot antenna elements were used to excite dual resonant modes.

The mutual coupling is decreased in [14] by using a metal boundary to achieve the stability of the boundary conditions of decoupling elements. Another method was used to mitigate the mutual coupling without any external decoupling structure as in [15]. This method is based on using compact tightly-arranged pairs. In [16], a self-isolated MIMO system uses three antennas, one T-shaped feeding element and two identical L-shaped radiating elements. The three antennas are symmetrically located along the central line of the antenna, where the two L-shaped elements act as decoupling element between two adjacent antenna units. In [17], the coupling was reduced by generating two orthogonally polarized waves. A compact and self-isolation was obtained by introducing two vertical stubs into the original antenna element as shown in [18]. On the other hand, the most popular frequency bands for the 5G applications in sub-six GHz band are N77 (3.3–4.2 GHz), N78 (3.3–3.8 GHz), N79 (4.4–5 GHz) and N48 (3.5–3.7 GHz) [19].

In this paper, a design of a wide band MIMO system is presented using 8 horizontal dual-loop antennas printed on the two sides of a smart phone board. The organization of the remaining parts of this paper is as follows. Section 2 presents the design of unit element antenna. The proposed design of the MIMO system is presented in Section 3. The MIMO parameters, envelope correlation coefficient (ECC), diversity gain (DG), and channel capacity loss (CLL) are calculated in Section 4. The effects of human hand and head on the MIMO system characteristics are depicted in Sections 5 and 6. All MIMO parameters are also studied for the two cases of the integration of the MIMO system with the hand and head of the human. The electromagnetic exposures into human head from the proposed MIMO antenna at two frequencies 3.5 GHz and 3.7 GHz are investigated and analyzed in terms of SAR in Section 7. Finally, simulated results of the proposed MIMO antenna are verified by comparing with experimental results in Section 8.

2. PROPOSED ELEMENT ANTENNA

The structure of the proposed unit element antenna is shown in Fig. 1. A dual-loop design is printed on the top and bottom sides of an FR4 substrate ($\varepsilon_r = 4.3$ and loss tangent $= 0.025$). The size of the substrate is $L_1 \times W_1$, and the thickness is 0.8 mm. The dimensions of antenna element are presented in Table 1. The loops dimensions are optimized to achieve the required bandwidth from 3.2 GHz to

Table 1. Dimensions of the single element.

Parameter	Value (mm)	Parameter	Value (mm)
W_1	50	L_4	10.25
L_1	37.5	L_5	3.1
L_2	25.5	S	5.7
L_3	21.75		

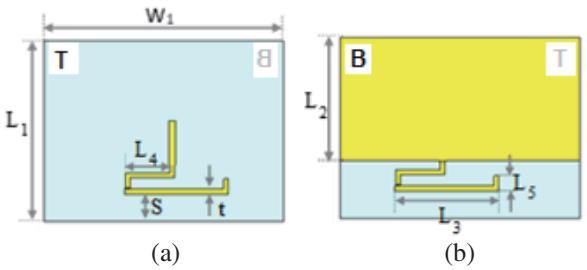

Figure 1. Element antenna design (a) top view and (b) bottom view.

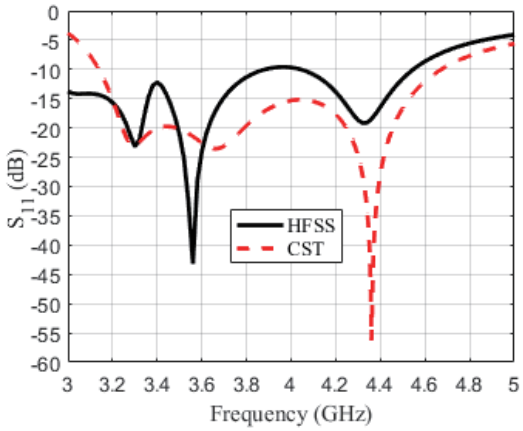

Figure 2. Reflection coefficient of element antenna.

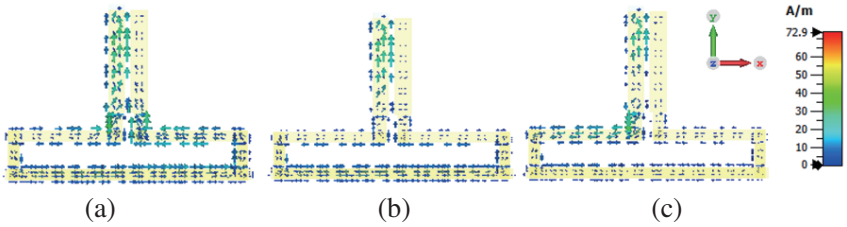

Figure 3. Current distribution of element antenna at (a) $f = 3.5\,\text{GHz}$, (b) $f = 3.7\,\text{GHz}$, and (c) $f = 4.6\,\text{GHz}$.

4.8 GHz. The partial ground plane size is $L_2 \times W_1$.

Figure 2 shows the reflection coefficient of the unit element antenna. It can be noted that the reflection coefficient for this antenna element is below $-6\,\text{dB}$ in the frequency range from 3.2 GHz to 4.8 GHz. The reflection coefficient of the proposed antenna is verified by two simulations, HFSS and CST. A good agreement between the two simulations is obtained. The radiation mechanism of the proposed antenna is further analyzed by investigating the surface current density. The surface current distribution is calculated at three resonance frequencies 3.5 GHz, 3.7 GHz, and 4.6 GHz. It can be noted that the current flow is mainly concentrated around the feed line as shown in Fig. 3. It can be noted that at 3.5 GHz, the current is nearly distributed over the two arms of the folded antenna. On the other hand, at 4.6 GHz the current is mainly concentrated on one half of the fed arm while the remaining parts of the antenna represent only parasitic elements.

3. DESIGN OF 8-ANTENNA MIMO SYSTEM

The top and bottom views of the proposed band 8-antenna MIMO system are shown in Fig. 4. The separation distance between the edges of adjacent antennas is $d_1 = 15.75\,\text{mm}$. The dimensions of the substrate are $L = 75\,\text{mm}$ and $W = 150\,\text{mm}$. On the other hand, the dimensions of the partial ground plane are $L_g = 51\,\text{mm}$ and $W_g = 134\,\text{mm}$. The eight antenna elements are arranged along the two side edges of the smartphone board. Each antenna element is fed by a $50\,\Omega$ microstrip line. For measurement purpose, these $50\,\Omega$ transmission lines are connected to SMA connectors. In practical case, these $50\,\Omega$ transmission lines are connected directly to the internal circuits of the handset. Fig. 5 shows the input reflection coefficients of these antenna elements in this arrangement. Due to the symmetry of the proposed MIMO antenna, two antenna elements are sufficient to obtain the results of all antenna elements. It can be noted that the obtained frequency band for this MIMO antenna where the input reflection coefficients of all its elements are below $-6\,\text{dB}$ extends from 3.2 GHz to 4.8 GHz which is quite useful for 5G sub-six GHz applications in the bands N77 (3.3–4.2 GHz), N78 (3.3–3.8 GHz), and N48

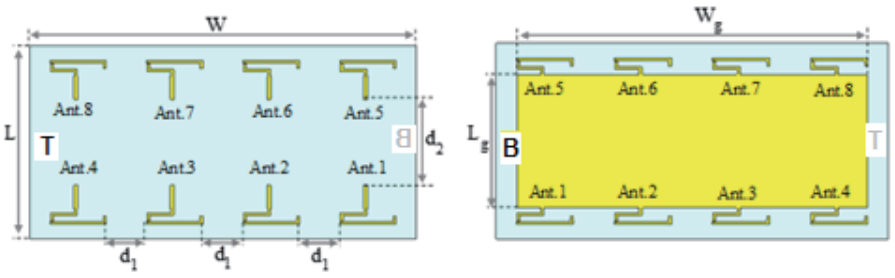

Figure 4. Eight antenna MIMO design (a) Top view, and (b) Bottom view.

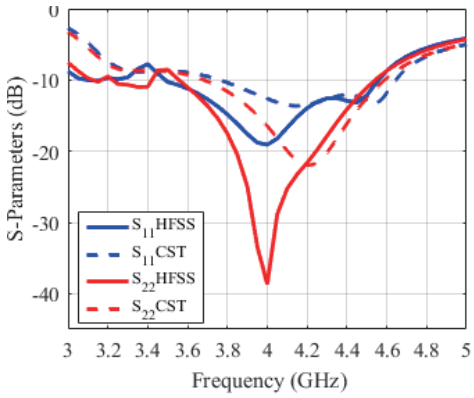

Figure 5. Simulated reflection coefficients of 8-antenna MIMO system.

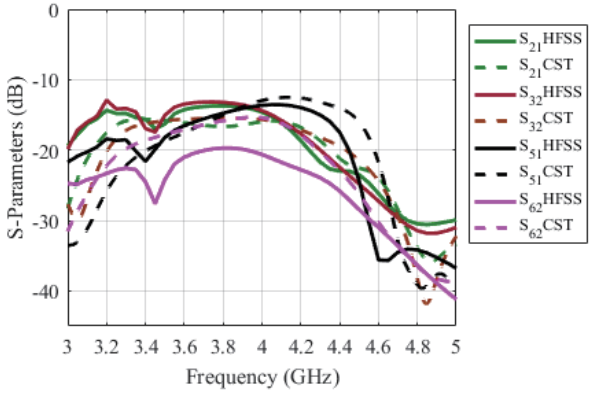

Figure 6. Simulated isolationcoefficients of 8-antenna MIMO system.

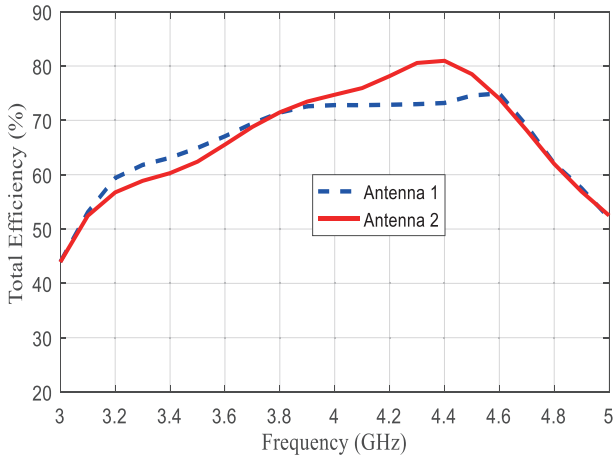

Figure 7. Simulated total efficiency for antenna 1 and antenna 2 of 8-antenna MIMO system.

(3.5–3.7 GHz). On the other hand, Fig. 6 shows isolation coefficients between the different elements of the MIMO system. It can be noted that the isolations between the different elements are below −14 dB in the proposed frequency band. The results are verified by using both HFSS and CST. Fig. 7 shows the total efficiency for antenna 1 and antenna 2 of the 8-antenna MIMO system. It can be noted from Fig. 7 that the total efficiency is greater than 55% in the entire band (3.2–4.8 GHz). Simulated 3D radiation patterns for antenna 1 and antenna 2 operating at 3.5 GHz and 3.7 GHz are shown in Fig. 8. It can be noted that both antennas have nearly omnidirectional radiation patterns.

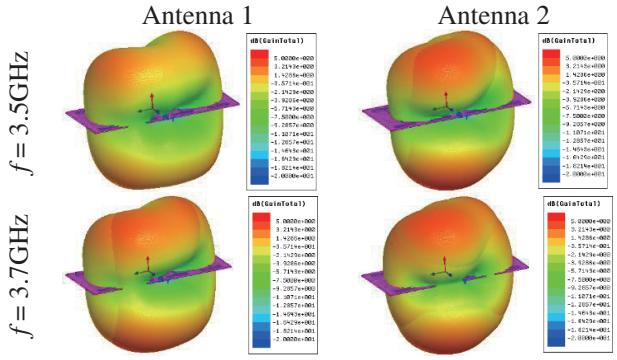

Figure 8. Simulated 3D radiation pattern for antenna 1 and antenna 2 operating at 3.5 GHz and 3.7 GHz.

4. MIMO PARAMETERS

Different parameters are analyzed to evaluate the performance of the multichannel antennas as envelope correlation coefficient (ECC), diversity gain (DG), and channel capacity loss (CLL).

4.1. Envelope Correlation Coefficient (ECC)

Envelope correlation coefficient is a measure of correlation between two separate antennas. ECC depends on the polarizations, the shape of the radiation pattern, the direction of the main beam, the phase shift between the two antennas, and other parameters. For the present case, the antenna elements have the same structure, and orientation ECCs can be calculated from the complex S-parameters of each antenna element in the MIMO system. The ECC between antenna i and antenna j can be calculated as follows [20].

$$\rho_{eij} = \frac{\left|S_{ii}^{*}S_{ij} + S_{ji}^{*}S_{jj}\right|^{2}}{\left(1 - |S_{ii}|^{2} - |S_{ji}|^{2}\right)\left(1 - |S_{jj}|^{2} - |S_{ij}|^{2}\right)} \tag{1}$$

For uncorrelated MIMO system, the value of ECC is 0 which represents the ideal value. The acceptable value for ECC is less than 0.5. The obtained ECCs for the proposed MIMO antenna are demonstrated in Fig. 9. The overall MIMO system indicates that the correlation values are less than 0.013 within operating bandwidth (3.2 GHz–4.8 GHz), which are all acceptable for the smart phone applications.

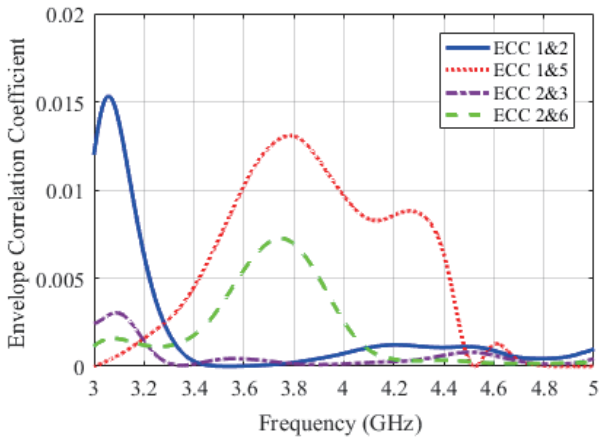

Figure 9. ECC of the proposed MIMO antenna.

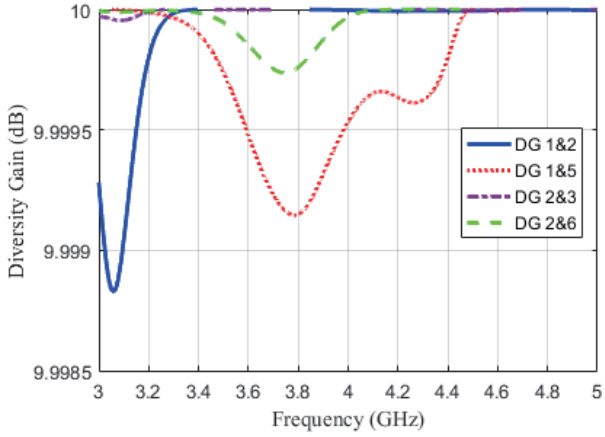

Figure 10. DG of the proposed MIMO antenna.

4.2. Diversity Gain (DG)

Diversity gain is how much the transmission power can be reduced when a diversity scheme is introduced, without a performance loss. The DG can be calculated as follows [20]:

$$DG = 10\sqrt{1 - |\rho_{eij}|^2} \tag{2}$$

The value of the DG should be about 10 dB for acceptable performance of MIMO system. Fig. 10 shows the DG of the proposed MIMO antenna. It can be noted that the DG demonstrates a good diversity performance of the antenna.

4.3. Channel Capacity Loss (CLL)

Channel capacity represents the percentage of information rate which can be transmitted through the channel without error. On the other hand, channel capacity loss (CCL) represents the percentage of this error. CLL can be calculated as follows [21]:

$$CCL = -\log_2 det\,(a) \tag{3}$$

where a is the correlation matrix, given by:

$$a = \begin{bmatrix} \sigma_{11} & \sigma_{12} \\ \sigma_{21} & \sigma_{22} \end{bmatrix} \tag{4}$$

$$\sigma_{ii} = 1 - \left(|S_{ii}|^2 - |S_{ij}|^2\right) \tag{5}$$

$$\sigma_{ij} = -\left(S_{ii}^* S_{ij} + S_{ji} S_{jj}^*\right) \tag{6}$$

Figure 11 shows the CCL of the proposed MIMO antenna. In the operating band (3.2 GHz–4.8 GHz), CLL value is less than 0.4 bit/s/Hz.

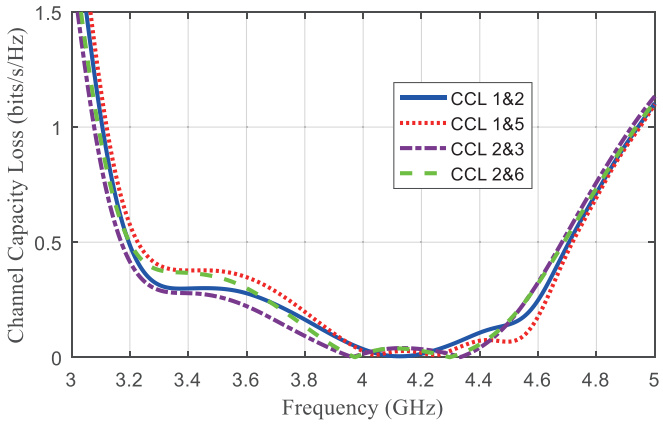

Figure 11. CLL of the proposed MIMO antenna.

5. INTERACTION OF MIMO ANTENNA WITH HUMAN HAND

In this section, the effect of human hand on the electrical performance of the MIMO system is discussed. CST human hand model integrated with the MIMO system is shown in Fig. 12. The reflection and isolation coefficients of the MIMO system integrated with human hand are plotted in Fig. 13. It is observed that integrating the human hand to the MIMO system does not decrease the matching band from 3.2 GHz to 4.8 GHz based on reflection coefficient below −6 dB. In additions, the isolation between different elements is still below −14 dB, except S_{51} which has a maximum value around −11 dB. Fig. 14 shows the total efficiency for antenna 1 and antenna 2 of the 8-antenna MIMO system integrated with human hand. The total efficiency is greater than 30% over the entire band (3.2–4.8 GHz).

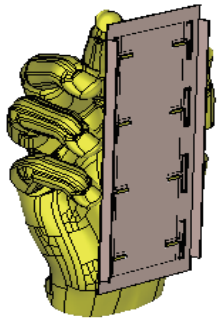

Figure 12. Simulation of 8-antenna MIMO system integrated with human hand.

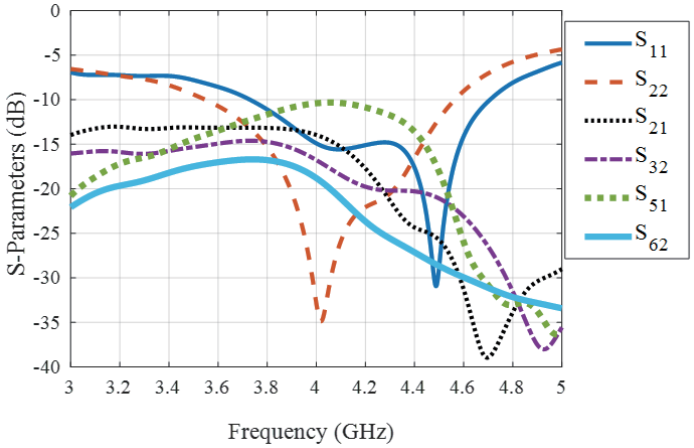

Figure 13. Simulated S-parameters of 8-antenna MIMO system integrated with human hand.

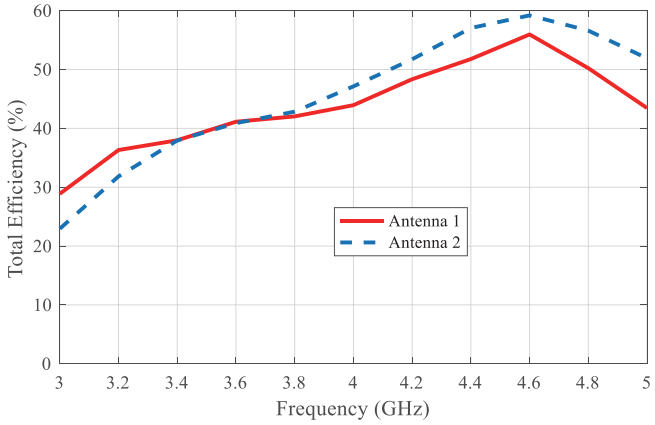

Figure 14. Simulated total efficiency of 8-antenna MIMO system integrated with human hand.

The simulated ECCs of 8-antenna MIMO system integrated with human hand are demonstrated in Fig. 15. The correlation values are less than 0.021 within operating bandwidth (3.2 GHz–4.8 GHz), which are still acceptable for smart phone applications. Fig. 16 describes the DG of the proposed MIMO antenna integrated with human hand. It can be noted that the DG demonstrates a good diversity performance of the antenna. In the operating band (3.2 GHz–4.8 GHz), the CLL value is less than 0.6 bit/s/Hz as shown in Fig. 17.

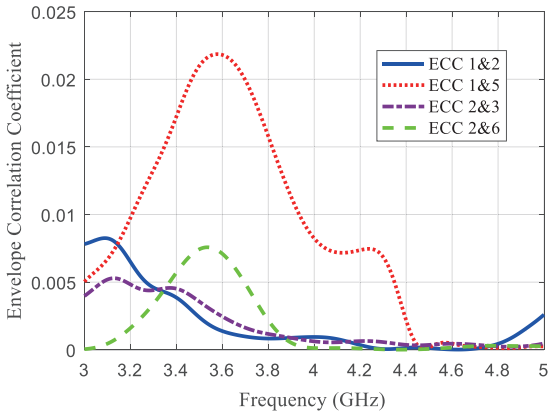

Figure 15. ECC of 8-antenna MIMO system integrated with human hand.

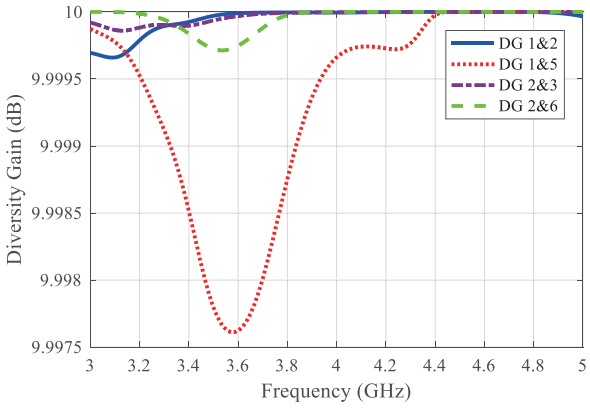

Figure 16. DG of 8-antenna MIMO system integrated with human hand.

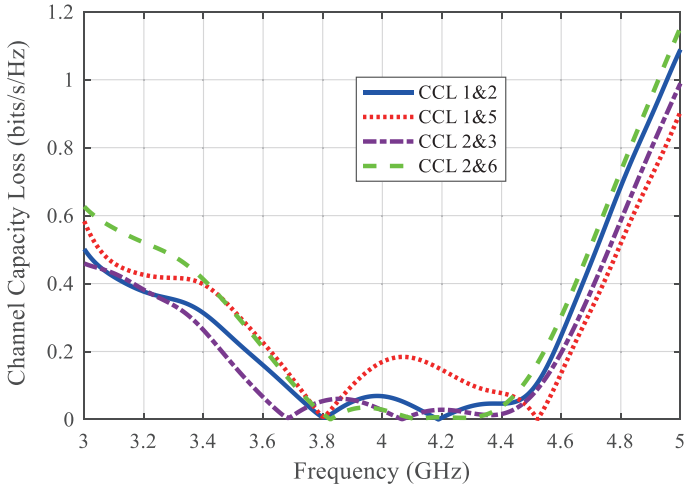

Figure 17. CCL of 8-antenna MIMO system integrated with human hand.

6. INTERACTION OF MIMO ANTENNA WITH HUMAN HEAD AND HAND

In this section, the effects of human head and hand on the performance of the MIMO antenna are investigated. CST human head and hand model integrated with the MIMO system is shown in Fig. 18. The reflection and isolation coefficients of the MIMO system integrated with human hand are shown

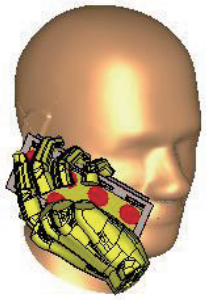

Figure 18. Simulation of 8-antenna MIMO system integrated with human head and hand.

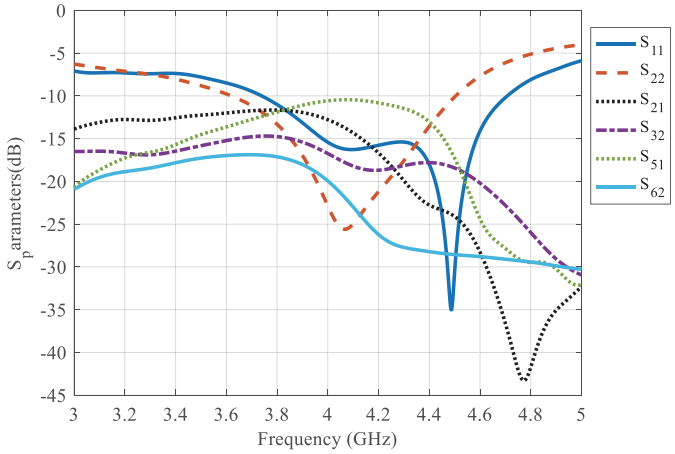

Figure 19. Simulated S-parameters of 8-antenna MIMO system integrated with human head and hand.

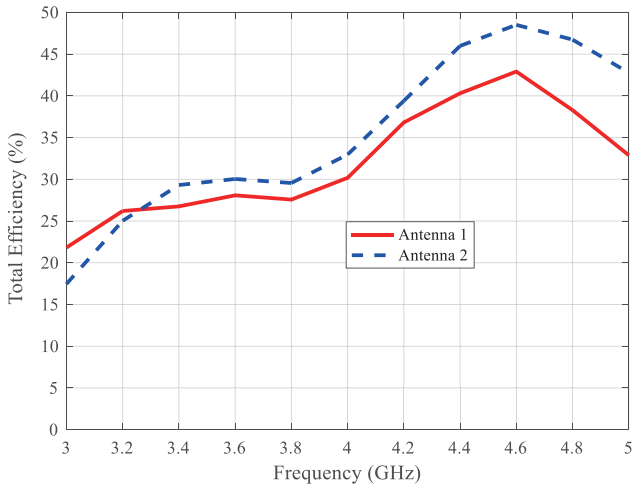

Figure 20. Simulated total efficiency of 8-antenna MIMO system integrated with human head and hand.

in Fig. 19. It can be noted that presence of the hand and head does not change the matching criteria in the frequency band from 3.2 GHz to 4.8 GHz to be below −6 dB. In addition, the isolation between the different elements is also below −14 dB, except S_{51} which is near −11 dB. Fig. 20 shows the total efficiency for antenna 1 and antenna 2 of the 8-antenna MIMO system integrated with human head and hand. The total efficiency in this case is greater than 25% in the entire band (3.2–4.8 GHz). It can be noted that the head and hand decrease the efficiency of the proposed MIMO antenna compared to the case in free space.

The simulated ECCs of 8-antenna MIMO system integrated with human head and hand are shown in Fig. 21. The correlation values in this case are less than 0.023 within operating bandwidth (3.2 GHz–4.8 GHz), which are still acceptable for the smart phone applications. Fig. 22 describes the DG of the proposed MIMO antenna integrated with human head and hand. It can be noted that the DG demonstrates a good diversity performance of the antenna. In the operating band (3.2 GHz–4.8 GHz), CLL is less than 0.6 bit/s/Hz as shown in Fig. 23. It is observed that the addition of the head and hand to the MIMO system has effects on the performance of the MIMO system compared to the case of free space. However, the performance of the MIMO system is still acceptable for smartphone applications.

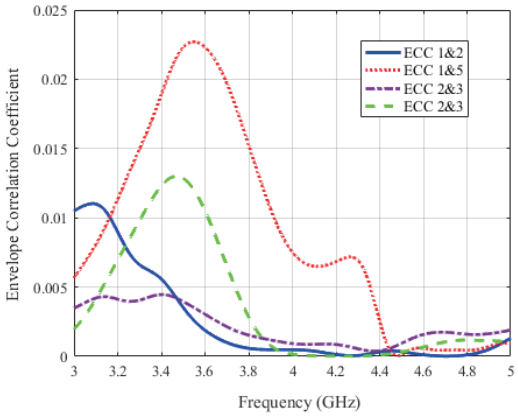

Figure 21. ECC of 8-antenna MIMO system integrated with human head and hand.

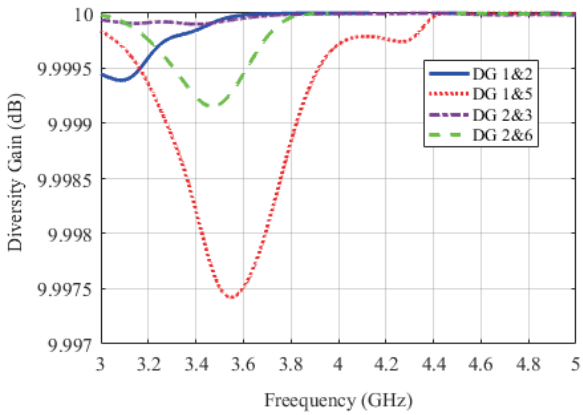

Figure 22. DG of 8-antenna MIMO system integrated with human head and hand.

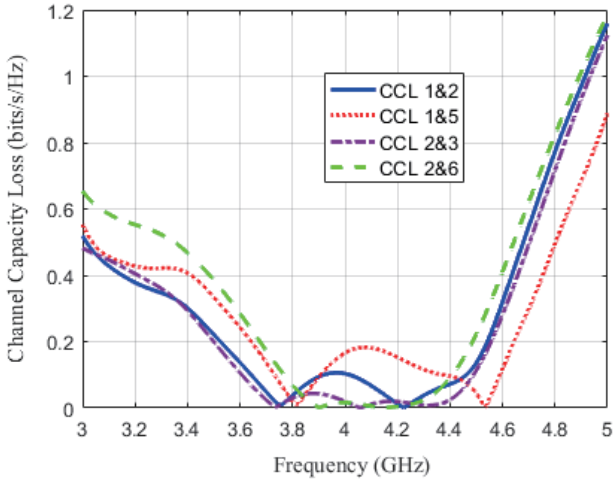

Figure 23. CLL of 8-antenna MIMO system integrated with human head and hand.

7. THE EFFECT OF THE MIMO SYSTEM ON THE HUMAN HEAD

Since the human body is always close to the antenna, the effect of the radiation from the antenna on the body should be examined, and the SAR distribution should be evaluated to ensure that it is below the acceptable level. The most frequently used specific absorption rate (SAR) limits are those of IEEE [22] which is 1.6 W/kg for any 1 g of tissue and ICNIRP (International Commission on Non-Ionizing Radiation Protection [23]) which is 2 W/kg for any 10 g of tissue.

Figure 24 shows the calculated SAR distribution along the human head for the MIMO antenna integrated with the human body at two different frequencies 3.5 GHz and 3.7 GHz. The obtained maximum SAR values for the MIMO antenna for 3.5 GHz and 3.7 GHz are 0.542 W/kg and 0.709 W/kg average over 10 g of tissue, respectively. It can be noted that the absorbed power in human head is less than 0.8 W/kg, and these values are much smaller than the allowable limits of SAR.

8. EXPERIMENTAL RESULTS AND DISCUSSION

A prototype of the proposed 8-antenna MIMO system was fabricated to verify the simulated results. Fig. 25 shows the fabricated MIMO system on the top and bottom views. For the measured operation, 8 SMA connectors were used. The reflection and isolation coefficients were measured using Agilent

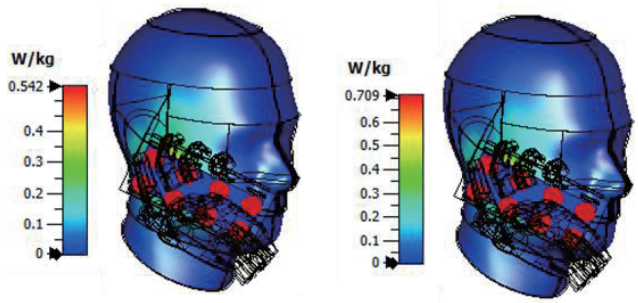

(a) (b)

Figure 24. SAR distribution at (a) $f = 3.5$ GHz and (b) $f = 3.7$ GHz.

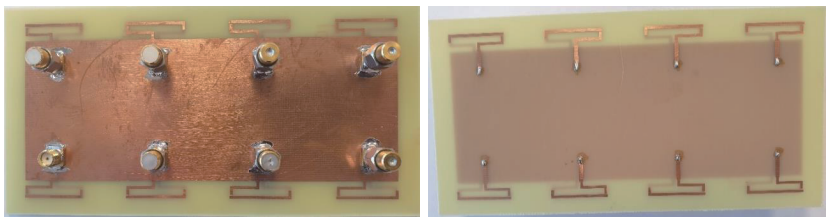

Figure 25. Fabricated of 8-antenna MIMO system.

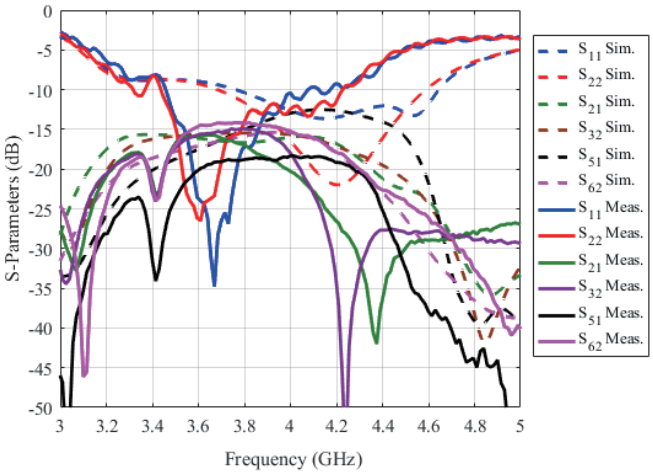

Figure 26. Simulated and measured S-parameters of 8-antenna MIMO system.

N9918A Vector Network Analyzer. Fig. 26 shows the measured versus simulated reflection and isolation coefficients. The measured reflection coefficients cover the band from 3.2 GHz to 4.4 GHz at −6 dB. It can be noted that the measured isolation coefficients between the adjacent antennas are better than the simulated isolation coefficients. The measured isolation between antennas 1 and 5 is less than −18 dB.

A comparison between simulated and measured ECCs is shown in Fig. 27. It is clear that the measured and simulated results are given a good performance in their behavior. Measured and simulated ECCs are less than 0.014 but are still less than the acceptable value (0.5). A good diversity gain is enhanced in Fig. 28. A good agreement between the simulated and measured diversity gains for all antennad. All the diversity gain values str around 10 dB in the operating band (3.2 GHz–4.8 GHz). On the other hand, simulated and measured CCLs are approximately identical in the lower band from 3 GHz to 4.2 GHz while there is a shift between them in the higher band from 4.2 GHz to 4.8 GHz as clear in Fig. 29. In conclusion from observing the comparison between the simulation and measurement

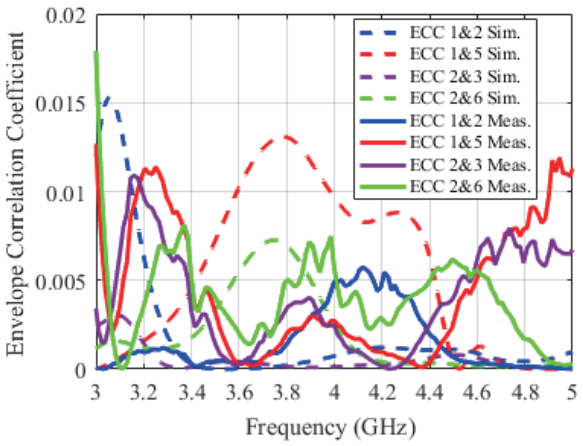

Figure 27. Simulated and measured ECC of 8-antenna MIMO system.

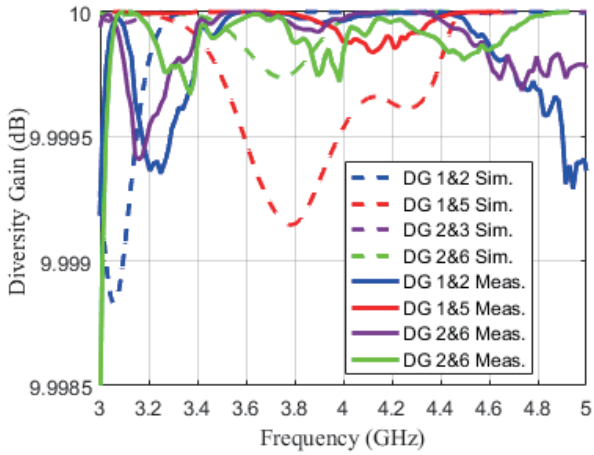

Figure 28. Simulated and measured DG of 8-antenna MIMO system.

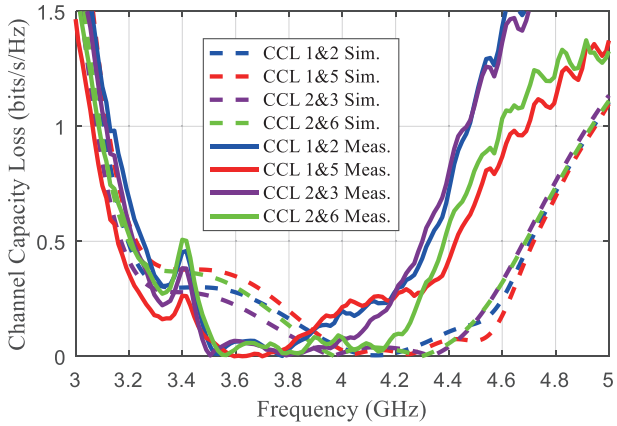

Figure 29. Simulated and measured CLL of 8-antenna MIMO system.

Table 2. Comparison with previous work.

	Bandwidth (GHz)	Isolation (dB)	Total efficiency%	ECC
Proposed MIMO Antenna	3.1–4.8 (−6 dB)	>14	60–80	<0.012
[24]	3.4–3.6 (−10 dB), 5.15–5.925 (−6 dB)	>12	50–56 and 53–65	<0.1 and <0.04
[25]	3.4-3.6 (−10 dB)	>10	62–68	<0.2
[26]	3.4–3.6(−6 dB)	>12	30–50	<0.3
[27]	3.4–3.6(−6 dB)	>10	40–52	<0.15
[28]	3.4–3.6 and 4.8–5.1 (−6 dB)	>11.5	41–74 and 40–85	<0.08 and <0.05
[29]	3.3–4.2 and 4.8–5 (−6 dB)	>11.5	53.8–76.5 and 62.6–79.1	<0.1 and <0.12

for all MIMO parameters ECC, DG, and CCL, there is a good performance for the MIMO system design in the operating band from 3.2 GHz to 4.8 GHz.

A comparison of the present design is performed with pervious 5G MIMO smartphone antennas. Previous published results focus on the band frequency from 3.6 to 4.6 GHz as in [25–27]. In [24, 28, 29], the system was designed with two narrow bands as in [24], operates at (3.4–3.6 GHz and 5.15–5.925 GHz); in [28], it operates at (3.4–3.6 GHz and 4.8-5.1 GHz); and in [29], it operates at (3.3–4.2 GHz and 4.8–5 GHz). The present design introduces a wide band antenna from 3.1 to 4.8 GHz, which covers 5G bands: N77, N78, and N48. The ECC of the present design is also less than 0.012. A good total efficiency is achieved in the article compared with the other published from 50–80%. The mutual coupling between the antennas is larger than 14 dB compared to other references in Table 2.

9. CONCLUSION

Eight dual-loop antennas are arranged horizontally to introduce a wide band MIMO system. Each dual-loop antenna is printed on both sides of the smart phone board. The dual-loop antenna covers the band from 3.2 GHz to 4.8 GHz at −6 dB. Two simulators, HFSS and CST, are used to verify the characteristics of the dual loop antenna. A good agreement between the two simulations is obtained. The surface current distribution is calculated at three resonance frequencies, 3.5 GHz, 3.7 GHz, and 4.6 GHz. The performance of the proposed MIMO system is verified by both simulation and measurement. A good performance of MIMO system is achieved. The reflection coefficients of the elements of the MIMO system are below −6 dB in the frequency band from 3.2 GHz to 4.4 GHz. The measured isolation coefficients between the adjacent antennas are better than the simulated isolation coefficients. The measured isolation between antennas 1 and 5 is less than −18 dB. The obtained MIMO parameters show low envelope correlation coefficient, good diversity performance, and low channel capacity loss. The coverage band of the proposed MIMO antenna is used for 5G applications: N77 (3.3–4.2 GHz), N78 (3.3–3.8 GHz), and N48 (3.5–3.7 GHz). The effect of human head and hand on the electrical performance of the MIMO system is studied. It is noted that the addition of the head and hand to the MIMO system has effects on its parameters compared to the case of MIMO antenna in free space. However, the total performance is still acceptable for smartphone applications. SAR distributions along the human head for the MIMO system integrated with the human body at two different frequencies 3.5 GHz and 3.7 GHz are reported. The maximum SAR values for the MIMO antenna for 3.5 GHz and 3.7 GHz are 0.542 W/kg and 0.709 W/kg average over 10 g of tissue, respectively. These values are much smaller than the allowable limits of SAR.

REFERENCES

1. Mak, K. M., H. W. Lai, K. M. Luk, and C. H. Chan, "Circularly polarized patch antenna for future 5G mobile phones," *IEEE Access*, Vol. 2, 1521–1529, Jan. 2015.
2. Al-Dulaimi, A., S. Al-Rubaye, Q. Ni, and E. Sousa, "5G communications race: Pursuit of more capacity triggers LTE in unlicensed band," *IEEE Vehicular Technology Magazine*, Vol. 10, No. 1, 43–51, Mar. 2015.
3. Chen, X., S. Shoaib, I. Shoaib, N. Shoaib, and C. G. Parini, "MIMO antennas for mobile handsets," *IEEE Antennas and Wireless Propagation Letters*, Vol. 14, 799–802, 2015.
4. Ban, Y.-L., C. Li, C.-Y.-D. Sim, G. Wu, and K.-L. Wong, "4G/5G multiple antennas for future multi-mode smartphone applications," *IEEE Access*, Vol. 4, 2981–2988, 2016.
5. Li, M. Y., Z. Q. Xu, Y. L. Ban, C. Y. D. Sim, and Z. F. Yu, "Eight-port orthogonally dual-polarised MIMO antennas using loop structures for 5G smartphone," *IET Microw., Antennas Propag.*, Vol. 11, 1810–1816, Dec. 2017.
6. Li, M.-Y., et al., "Eight-port orthogonally dual-polarized antenna array for 5G smartphone applications," *IEEE Trans. Antennas Propag.*, Vol. 64, No. 9, 3820–3830, Sep. 2016.
7. Tsai, C.-Y., K.-L. Wong, and W.-Y. Li, "Experimental results of the multi-Gbps smartphone with 20 multi-input multi-output (MIMO) antennas in the 20–12 MIMO operation," *Microw. Opt. Technol. Lett.*, Vol. 60, 20012010, Aug. 2018.

8. Wong, K.-L., C.-Y. Tsai, and J.-Y. Lu, "Two asymmetrically mirrored gap-coupled loop antennas as a compact building block for eight-antenna MIMO array in the future smartphone," *IEEE Trans. Antennas Propag.*, Vol. 65, No. 4, 1765–1778, Apr. 2017.
9. Deng, J. Y., J. Yao, D. Q. Sun, and L. X. Guo, "Ten-element MIMO antenna for 5G terminals," *Microw. Opt. Technol. Lett.*, Vol. 60, 3045–3049, Dec. 2018.
10. Wong, K. L., B. W. Lin, and W.-Y. Li, "Dual-band dual inverted-F/loop antennas as a compact decoupled building block for forming eight 3.5/5.8-GHz MIMO antennas in the future smartphone," *Microw. Opt. Technol. Lett.*, Vol. 59, 2715–2721, Nov. 2017.
11. Guo, J., L. Cui, C. Li, and B. Sun, "Side-edge frame printed eight-port dual-band antenna array for 5G smartphone applications," *IEEE Trans. Antennas Propag.*, Vol. 66, 7412–7417, Dec. 2018.
12. Li, Y., C. Y. D. Sim, Y. Luo, and G. Yang, "12-port 5G massive MIMO antenna array in sub-6 GHz mobile handset for LTE bands 42/43/46 applications," *IEEE Access*, Vol. 6, 344–354, Feb. 2018.
13. Li, Y., C.-Y.-D. Sim, Y. Luo, and G. Yang, "Multiband 10-antenna array for sub-6 GHz MIMO applications in 5-G smartphones," *IEEE Access*, Vol. 6, 28041–28053, Jun. 2018.
14. Xu, H., H. Zhou, S. Gao, H. Wang, and Y. Cheng, "Multimode decoupling technique with independent tuning characteristic for mobile terminals," *IEEE Trans. Antennas Propag.*, Vol. 65, No. 12, 6739–6751, Dec. 2017.
15. Sun, L. B., H. Feng, Y. Li, and Z. Zhang, "Compact 5G MIMO mobile phone antennas with tightly arranged orthogonal-mode pairs," *IEEE Trans. Antennas Propag.*, Vol. 66, No. 11, 6364–6369, Nov. 2018.
16. Zhao, A. and Z. Ren, "Multiple-input and multiple-output antenna system with self-isolated antenna element for fth-generation mobile terminals," *Microw. Opt. Technol. Lett.*, Vol. 61, 20–27, Jan. 2019.
17. Li, M.-Y., Y.-L. Ban, Z.-Q. Xu, J. Guo, and Z.-F. Yu, "Tri-polarized 12-antenna MIMO array for future 5G smartphone applications," *IEEE Access*, Vol. 6, 6160–6170, Jan. 2018.
18. Zhao, A. and Z. Ren, "Size reduction of self-isolated MIMO antenna system for 5G mobile phone applications," *IEEE Antennas Wireless Propag.Lett.*, Vol. 18, No. 1, 152–156, Jan. 2019.
19. https://en.wikipedia.org/wiki/5G_NR_frequency_bands.
20. Sharawi, M. S., "Printed multi-band MIMO antenna systems and their performance metrics [wireless corner]," *IEEE Antennas and propagation Magazine*, Vol. 55, No. 5, 218–232, 2013.
21. Khalid, M., S. Naqvi, N. Hussain, M. Rahman, S. Mirjavadi, et al., "4-Port MIMO antenna with defected ground structure for 5G millimeter wave applications," *Electronics*, Vol. 9, 2020.
22. "IEEE standards for safety levels with request to human exposure to radiofrequency electromagnetic fields, 3 kHz to 300 GHz," IEEE Std. C95.1, 1999.
23. ICNIRP (International Commission on Non-Ionizing Radiation Protection), "Guidelines for limiting exposure to time-varying electric magnetic, and electromagnetic fields (up to 300 GHz)," *Health Phys.*, Vol. 74, 494–522, 1998.
24. Zou, H., Y. Li, C.-Y.-D. Sim, and G. Yang, "Design of 8_8 dual-band MIMO antenna array for 5G smartphone applications," *Int. J. RF Microw. Comput. Aided Eng.*, Vol. 28, No. 9, Art. No. e21420, Nov. 2018.
25. Ban, Y. L., C. Li, C. Y. D. Sim, G. Wu, and K. L. Wong, "4G/5G multiple antennas for future multi-mode smartphone applications," *IEEE Access*, Vol. 4, 2981–2988, 2016.
26. Wong, K. L., J. Y. Lu, L. Y. Chen, W. Y. Li, and Y. L. Ban, "8-antenna and 16-antenna arrays using the quad-antenna linear array as a building block for the 3.5-GHz LTE MIMO operation in the smart-phone," *Microw Opt Technol Lett.*, Vol. 58, 174–18, 2016.
27. Wong, K. L., C. Y. Tsai, and J. Y. Lu, "Two asymmetrically mirrored gap-coupled loop antennas as a compact building block for eight-antenna MIMO array in the future smartphone," *IEEE Trans. Antennas Propag.*, Vol. 65, 1765–1778, 2017.
28. Guo, J. L., L. Cui, C. Li, and B. H. Sun, "Side-edge frame printed eight-port dual-band antenna array for 5G smartphone applications," *IEEE Trans. Antennas Propag.*, Vol. 66, No. 12, 7412–7417, Dec. 2018.

29. Cui, L., J. Guo, Y. Liu, and C.-Y.-D. Sim, "An 8-element dualband MIMO antenna with decoupling stub for 5G smartphone applications," *IEEE Antennas Wireless Propag. Lett.*, Vol. 18, No. 10, 2095–2099, 2019.